

Digital nanoreactors to control absolute stoichiometry and spatiotemporal behavior of DNA receptors within lipid bilayers

Received: 28 September 2022

Accepted: 24 February 2023

Published online: 20 March 2023

 Check for updates

Vishal Maingi¹✉, Zhao Zhang², Chris Thachuk³✉, Namita Sarraf¹,
Edwin R. Chapman²✉ & Paul W. K. Rothmund^{1,4,5}✉

Interactions between membrane proteins are essential for cell survival but are often poorly understood. Even the biologically functional ratio of components within a multi-subunit membrane complex—the native stoichiometry—is difficult to establish. Here we demonstrate digital nanoreactors that can control interactions between lipid-bound molecular receptors along three key dimensions: stoichiometric, spatial, and temporal. Each nanoreactor is based on a DNA origami ring, which both templates the synthesis of a liposome and provides tethering sites for DNA-based receptors (modelling membrane proteins). Receptors are released into the liposomal membrane using strand displacement and a DNA logic gate measures receptor heterodimer formation. High-efficiency tethering of receptors enables the kinetics of receptors in 1:1 and 2:2 absolute stoichiometries to be observed by bulk fluorescence, which in principle is generalizable to any ratio. Similar single-molecule-in-bulk experiments using DNA-linked membrane proteins could determine native stoichiometry and the kinetics of membrane protein interactions for applications ranging from signalling research to drug discovery.

Many cellular functions are mediated by signalling events triggered by protein-protein encounters occurring within lipid bilayer membranes¹. Understanding membrane protein interactions and their downstream effects often provide direct and important insight into how cells function on the molecular level. Membrane protein interactions trigger countless cascades of events essential to cellular function, yet for many membrane proteins, we lack even a basic understanding of what structural arrangement is necessary to trigger these events. However, it is often difficult to establish whether the active form of an integral membrane protein is a monomer or oligomer (a complex containing two or more interacting partners), or which of many potential homomeric or heteromeric complexes is physiologically relevant². Basic characterization of the biologically active oligomeric state of

membrane proteins is a prerequisite to understanding their function^{3–5} and is useful for drug discovery^{6,7}, dissecting the molecular mechanism of pathogenic processes⁸, and elucidating the role of transient membrane protein interactions⁹.

Existing experimental approaches for characterization of the oligomeric state each have their limitations: polyacrylamide gel electrophoresis cannot replicate the native lipid environment and can itself introduce artifactual dimers¹⁰; chemical cross-linking can be employed to stabilize oligomers under non-native conditions at the risk of introducing artifactual dimers from nonspecific reactions¹¹; bulk Förster resonance energy transfer (FRET) data is concentration sensitive, and must be carefully corrected to account for potential FRET between oligomers¹², single-molecule fluorescence photobleaching and FRET

¹Department of Bioengineering, California Institute of Technology, Pasadena, CA, USA. ²Department of Neuroscience and Howard Hughes Medical Institute, University of Wisconsin-Madison, 1111 Highland Avenue, Madison, WI 53705, USA. ³Paul G. Allen School of Computer Science & Engineering, University of Washington, Seattle, WA, USA. ⁴Department of Computation & Neural Systems, California Institute of Technology, Pasadena, CA, USA. ⁵Department of Computation + Mathematical Sciences, California Institute of Technology, Pasadena, CA, USA. ✉e-mail: maingivishal@gmail.com; thachuk@cs.washington.edu; chapman@wisc.edu; pwkr@dna.caltech.edu

methods can exquisitely resolve features of oligomers but are technically challenging^{11–16}, and mass spectrometry requires detergents for sample preparation and expensive instrumentation¹⁷. Often, to definitively characterize the oligomeric state, it is necessary to combine multiple analytical approaches, adding time and complexity. An ideal experimental platform for membrane protein interactions would avoid the drawbacks of the methods above, enable the study of isolated proteins in a cell-free yet native lipid environment, and measure real-time kinetics and dynamics of their interactions. Further, the platform would simultaneously provide precise stoichiometric, spatial, and temporal (S²T) control: exact numbers of monomeric proteins would begin in a well-separated initial configuration within a well-defined reaction volume, and their triggered release could be used to time the beginning of the experiment.

One path to such an ideal platform is DNA nanotechnology, which has recently been used to construct a number of custom instruments for biology^{18–25} wherein DNA nanostructures are designed from the beginning to ask exactly the experimental question at hand. The construction of custom molecular instruments has been enabled by the versatility of DNA nanotechnology: DNA can be folded²⁶ or assembled into 2D^{27,28} or 3D^{29,30} shapes, these shapes can be programmed to create reconfigurable devices and machines³¹, and can be decorated with a variety of functional groups, e.g., proteins³² and polymers³³, whose position can be controlled in 0.34 nm steps. This has enabled S²T control in the context of surface chemical reaction networks on DNA origami^{34–38}, where reactants hop from one periodic lattice site to the next. Critical to extending S²T control to fluid bilayers are commercially available and custom-made hydrophobic modifications to that interface DNA with lipid membranes: they have been used by many research groups to engineer and study DNA-lipid systems^{39–41} with applications varying from artificial nanopores^{42,43}, to membrane sculpturing⁴⁴, nanodiscs^{45–47}, DNA circuits^{48–51}, control of liposome fusion^{52–57}, and artificial cells⁵⁸. Yet so far, no such system has achieved full S²T control on a lipid bilayer.

Here, our approach is to use DNA nanotechnology to build a hybrid DNA-lipid instrument, a DNA Origami-templated Liposome (DOL)³⁹, which provides a generic assay platform to orchestrate and measure the interactions between reacting species in a single lipid bilayer. To validate our platform, we use membrane-anchored DNA complexes, which we term DNA receptors, as models for membrane proteins (actual membrane proteins are not used in this work). We exploit several strategies to create a membrane-based platform that achieves full S²T control. First, we use a well-defined and addressable structure of DNA origami²⁷ nanocage⁵⁹ to exert absolute stoichiometric^{60–62} and spatial control over the DNA receptors. Building on previous work^{39,59} which demonstrates that guest liposomes of well-defined size can be templated within DNA origami cages, we arrange discrete numbers (e.g. two or four) of DNA receptors at precise distances (e.g., 45 nm) along the circumference of a liposome-filled cage to create a well-defined initial state (Figs. 1a and 1b, Step 1). Cholesterol on the DNA receptors binds them to the liposome, and tethers between the receptors and the cage serve to protect them and keep them from reacting until desired. Next, we use toehold-mediated strand displacement (TMSD^{63–65}) to both provide temporal control via triggered reaction initiation (Fig. 1a, b, Step 2) and to create a DNA logic gate⁶³ that outputs a fluorescent signal to measure the extent of DNA receptor heterodimerization (Fig. 1a, b, Step 3). Because the logic gate requires simultaneous interaction of both receptors with a reporter complex, our system models a ligand-induced protein dimerization process. Measurement of DNA receptor interaction kinetics for two different absolute stoichiometries, both on the DOL and in solution, show that: (1) we achieve digital control over the number of receptor complexes localized to the DOL, (2) receptors interact primarily within a single DOL rather than between DOL, and (3) DOL-bound receptors react with an effective rate constant that is

2800-fold higher than that measured in solution. Thus, DOL can be thought of as digital nanoreactors—defining, isolating, and concentrating reactions between membrane-bound receptors; where digital signifies the copy number of receptors and nanoreactor signifies the localization of reaction on a single DOL.

Results

The DOL platform

Figure 1a summarizes our DOL synthesis strategy (Fig. 1a left) and its use for controlling DNA receptor interactions (Fig. 1a right, Supplementary Figure 1). A pool of staple strands, including special staples with linker extensions, was annealed with a circular DNA scaffold (Step A) to assemble a cage-like DNA origami comprising two interconnected rings; here we refer to this entire structure simply as a ring. The linker-extended staples were designed to specify the number, position, and type of DNA receptors that were attached to the ring in the next step. In particular, the sticky end overhangs presented by each linker determine which receptor type will bind at a particular position on the ring. Two linkers are shown in Fig. 1a, suitable for 1:1 receptor absolute stoichiometry; four linkers were used for 2:2 receptor absolute stoichiometry. To remove excess staples and undesired higher-order structures, the reaction products were purified via rate-zonal ultracentrifugation (separating by size, Supplementary Figure 1b). Next, preformed DNA receptors were attached to the rings by an isothermal incubation (Step B); excess receptors were removed in a second rate-zonal ultracentrifugation (Supplementary Figure 1c). Additionally, at least thirty staples on the ring, termed handles, carry extensions designed to bind complementary cholesterol-modified DNA strands termed anti-handles. Anti-handles were attached to rings in a second isothermal incubation (Step C). The cholesterol-modified rings, with tethered receptors, were next mixed with lipids and detergents (Step D). During a follow-up detergent removal process, the cholesterol modifications served as seed for the formation of a liposome inside the ring, creating DOL. The resultant mixture, containing undesired free liposomes and DOL, were purified using isopycnic ultracentrifugation (separating by density, Supplementary Figure 1d). Fractions containing fully assembled DOL (see Supplementary Note 1) were used to analyze DNA receptor interactions.

DNA receptors and their interaction logic

Figure 1b and Table 1 show the domain-level representation of our two different types of DNA receptor complexes (Receptor_A and Receptor_B). We explain domain-level details for Receptor_A; Receptor_B has the same domain-level structure, but with different sequences. Supplementary Table 1 more extensively describes domains and their roles. Sequence design and analysis were done with NUPACK⁶⁶, which employs SantaLucia nearest-neighbor parameters⁶⁷, assuming 1 M Na⁺ at 25 °C and using default dangle parameters.

Receptor_A is composed of two cholesterol-modified oligonucleotides, anchor_A and anchor_A*. Domain A (in anchor_A) is complementary to domain A* (the only domain in anchor_A*); together these domains serve the purpose of membrane anchoring via their cholesterol modifications. In general, the use of two cholesterol provides a more stable association of DNA complexes with membranes than does a single modification^{49,54}. Further, DOL lipid phase and the buffer conditions favor cholesterol anchor mediated DNA-lipid binding instead of ion-mediated bridging effect⁶⁸ (see related discussion in Supplementary Note 2b). PIX2 in anchor_A hybridizes with P1*X2* in linker_A (an extension from a staple strand in the ring) which tethers the receptor to the ring during DOL assembly (Step B, Fig. 1a). After synthesis, in Step 1 (Fig. 1b), receptors are separated on the ring by ~45 nm.

In Step 2, addition of release_A strand, results in TMSD release of Receptor_A, as initiated by the hybridization of domain T with toehold T* on linker_A. The subsequences TP1X2 (release_A) and X2*P1*T*

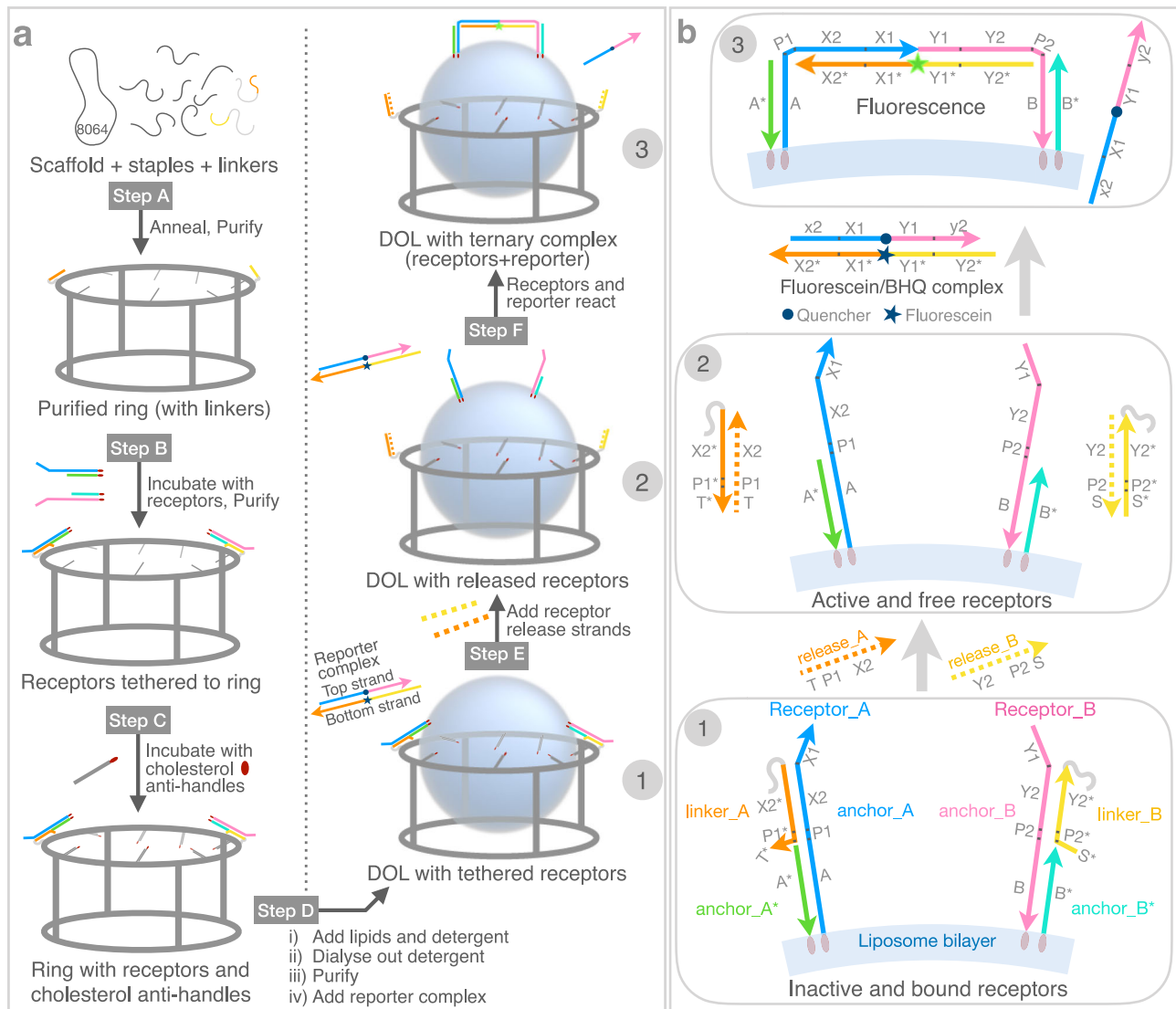


Fig. 1 | DOL synthesis and DNA circuit logic. **a** DOL assembly (left column) and DNA receptor interaction (right column). Step A: DNA scaffold (8064 nucleotides; gray loop), regular staple strands (gray segments), and linker-extended staples (having orange and yellow sections) were annealed; excess staples were removed. Step B: Two types of DNA receptors modified with cholesterol (red ovals) were tethered to the ring and rings were purified. Step C: Rings were incubated with cholesterol-modified anti-handles (gray lines with red ovals). Step D: Lipids and detergent were added; subsequent dialysis removed detergent and seeded liposome formation (blue spheres) on rings to create DOL. **b** Stepwise operation of a DNA circuit for the receptor release and interaction measurement. Step labels 1–3 correspond to labels in the right column of **a**. A zoomed segment of the liposome bilayer is shown. Initially (Step 1) both receptors are inactive and bound to the ring

(not shown) via linker_A and linker_B (themselves attached to the ring via a short section of gray polyT). The inter-receptor distance (~45 nm) is not shown to scale. Receptors were detethered (Step 2) by adding release strands complementary to the linkers; domains T* and S* provided footholds for this reaction. Released receptors diffuse freely within the bilayer but do not interact. Receptor interaction (Step 3) is mediated by a reporter complex consisting of a top strand with internal quencher (dark blue circle) and a bottom strand with an internal fluorophore (star; dark blue when quenched or green when fluorescent). Table 1 gives domains and sequences for all circuit components. DNA domains shown in different colors in **b** have a specific role as explained in Supplementary Table 1. DOL; DNA origami liposome, BHQ; black hole quencher.

(linker_A) are fully complementary, and thus their full hybridization, after TMSD of PIX2, is thermodynamically more favorable and essentially irreversible. The released Receptor_A has a free unpaired subsequence PIX2X1 and, similarly, after the addition of release_B, the Receptor_B has an unpaired Y1Y2P2 subsequence. By design, PIX2X1 (NUPACK-calculated free energy $\Delta G^\circ = -0.27$ kcal mol⁻¹; shows little predicted secondary structure) and Y1Y2P2 (NUPACK-calculated free energy $\Delta G^\circ = 0$; unstructured) is not predicted to hybridize (NUPACK reports no bound complex at experimentally relevant concentrations); thus, released Receptor_A and Receptor_B are unlikely to interact with each other.

Released receptors can only interact (Step 3) in the presence of a reporter complex (ligand), which is a fluorophore-quenched

duplex comprising a top strand containing an internal quencher (black hole quencher; BHQ) and a bottom strand containing an internal fluorophore (fluorescein). The bottom strand of the reporter ($Y2^*Y1^*X1^*X2^*$) has two five-nucleotide footholds: $X2^*$ initiates binding of Receptor_A to reporter via $X2$ in anchor_A and $Y2^*$ initiates binding of Receptor_B to reporter via $Y2$ in anchor_B. Overall, the formation of a ternary complex by Receptor_A, Receptor_B, and the reporter's bottom strand is very similar to the cooperative hybridization reaction reported by Zhang⁶⁹ which represents an AND gate where Receptor_A and Receptor_B are inputs and the ternary complex is an output. Note that intermediate states formed by either receptor individually with the reporter complex (i.e. states Aⁱ and Bⁱ in Supplementary Figure 2) are thermodynamically less favorable than the reactants, and thus

Table 1 | Domain-level sequences (5'–3') of two different types of DNA receptor and reporter complexes

Domain	Sequence
A* (anchor_A*)	GTTTGAGTTGAGTGGGAAAG/3CholTEG/
A.P1.X2.X1 (anchor_A)	/5Chol-TEG/CTTTCCCACTCAACTCAAAC. CA. ACACCATTACCAC. ATTCAAATCC
X2*.P1*.T* (linker_A)	GTGGGTAAATGGTGT. TG. AGATG
B* (anchor_B*)	/5Chol-TEG/GTTGGTAATGGAATGGGAAAG
Y1.Y2.P2.B (anchor_B)	CACAATACAC. CCTACACATACATCA. AC. CTTCCTCCATTCCATTACCAAC/3CholTEG/
S*.P2*.Y2* (linker_B)	GTGGA. GT. TGATGTATGTGTAGG
T.P1.X2 (release_A)	CATCT. CA. ACACCATTACCAC
Y2.P2.S (release_B)	CCTACACATACATCA. AC. TCCAC
x2.X1.Y1.y2 (reporter top strand)	atttaccac. ATTCAAATCC. /iBHQ-1dT/. CACAATA-strand
Y2*. Y1*. X1*. X2*(reporter bottom strand)	TGATGTATGTGTAGG. GTGTATTGTG. /iFluorT/. GGATTGAAT. GTGGTAAATGGTGT

See Fig. 1 for domain-level diagrams of different complexes and Supplementary Table 1 (showing color codes corresponding to the same colored domains shown in Fig. 1) for more extensive description of domains and their roles. iBHQ-1dT (IDT commercial code) is a black hole quencher and iFluorT (IDT commercial code) is a fluorescein and both conjugated to internal T nucleotides, Chol-TEG is a TEG-linked cholesterol molecule (IDT commercial code). Note that domains labeled with lower case are partially complementary to their upper-case counterparts. E.g. x2 (reporter top strand) is a shortened version of X2 and is only partially complementary to X2* (reporter bottom strand). Note that the sequences for the gray domains of the linker strands shown in Fig. 1 are not provided here (see Supplementary Data 2 for the full-length sequences of linker strands). Source data are provided as a Source Data file.

sequester very little of either receptor⁶⁹. Further, the formation of intermediate states, which are kinetically reversible, does not result in dequenching of the fluorophore (Fig. 3, discussed below). Successful dequenching of the reporter complex (and resulting fluorescence) is only possible when both the receptors are present to cooperatively displace the BHQ-containing top strand. P1 and P2 domains of the ternary complex remain unpaired, acting as flexible hinges.

Intra-DOL receptor interactions

Implementing the DNA logic gate shown in Fig. 1b, we explain here interactions between two receptors, one Receptor_A and one Receptor_B per DOL (DOL^{1A1B}), initially tethered at distal ends of the ring and anchored in the liposome membrane with their cholesterol ends (Fig. 2a, left). To set up a plate reader experiment, the reporter complex (final concentration 4.7 nM) was first mixed with purified DOL^{1A1B} fraction and then the fluorescence intensity was initially measured for ~7 h (Fig. 2d, blue curve). No increase in fluorescence was observed during this phase because the lipid-anchored receptors remain inactive and tethered to the ring via linker strands. Note that linker strands serve the dual purpose of tethering as well as protecting the reactive domains of the receptors. This initial period (7 h) of measurement served as a quality check of our overall purification process. If our purification method of getting rid of untethered reactive receptors was not successful, we would expect to see a rise in signal during this phase. Any unbound and thus active receptors, possibly in solution or on DOL, with their reacting domains PIX2X1 (in anchor_A) and Y1Y2P2 (in anchor_B) can interact with the reporter complex in solution to generate fluorescence. But no significant change in fluorescence was observed, indicating that our purification protocol successfully removed most of the unbound excess receptors (see related discussion in Supplementary Note 2a).

After 7 h, a mix of release_A and release_B (both at 100 nM final concentration) was added, which triggered the release of both receptors on the surface of lipid bilayer. Through cooperative hybridization, both the active receptors react with the reporter complex to completely displace the BHQ top strand forming one ternary complex per DOL (Fig. 2a, right). As a result, a quick rise in fluorescence was

observed which almost saturated within ~3.5 h of releasing the receptors. Similarly, using the same DOL platform but with two additional linkers, we studied another case where two Receptor_A and two Receptor_B were tethered per DOL which form two ternary complexes per DOL (DOL^{2A2B}, Fig. 2b). Figure 2d, orange curve, shows the fluorescence kinetics for DOL^{2A2B} case. In all the cases, here and other cases discussed later, to determine whether all the reporter complex has been consumed or not, excess of anchor_A and anchor_B strands (without cholesterol modifications, and 100 nM final concentration for each) was added, evident as a quick spike in fluorescence, and then the fluorescence was measured for another 4 to 6 h. This helped us to normalize the data and also this procedure provides an indirect way to measure DOL concentration by knowing the fraction of reporter consumed (Supplementary Note 3). Thus, in all these cases, the fluorescence saturation achieved at c.a. 36 h is related to the reporter complex consumed by receptors present on DOL, and is thus dependent on the DOL concentration in a particular fraction used for analyses as explained further.

We also explored the situation where two types of receptors were tethered to two rings, which later dimerized and together templated a liposome (Supplementary Note 5, Supplementary Figures 7 and 8). Similar to the above cases, both receptors were released on the template liposome bilayer and fluorescence was measured in the presence of reporter complex (Fig. 2c, d). The dimer platform demonstrates that reactants can come from two different rings, which could be potentially suitable for specific applications.

Inter-DOL receptor interactions

The main purpose of the DOL platform is to control and quantify single-molecule isolated interactions between receptors on the same lipid bilayer surface (intra-DOL) with minimal cross-talk among the DOLs in-bulk solution. Thus, it is essential to determine any contribution originating from one receptor interacting with the other on two different DOLs (inter-DOL). We created DOL having only a single type of receptor, which allowed us to study receptor interactions purely as inter-DOL reactions. For example, to evaluate possible inter-DOL interactions in the case of DOL^{1A1B} (intra-DOL) we assembled DOL^{1A} and DOL^{1B} individually, and then mixed (referred to as interDOL^{1A1B}) equal volumes of their purified fractions (pooled fractions 3 + 4 each case), and performed similar plate reader measurements as described above for intra-DOL cases. Overall, Fig. 2e shows that the inter-DOL reaction rate is slower than the intra-DOL interaction. This implies that most of the fluorescence signal obtained in the intra-DOL case, which has faster reaction kinetics, is due to receptors anchored on the same surface. Similarly, comparing inter-DOL interaction of DOL^{2A} and DOL^{2B} (interDOL^{2A2B}) with intra-DOL DOL^{2A2B} faster kinetics was observed in DOL^{2A2B} (Figs. 2d and 2e). The correlated noise observed in Fig. 2e curves is due to the instrument itself (light source), samples were run at the same time and data was subtracted from the same blank reference.

Kinetics

Figure 2d–f show kinetics curves for receptor interactions occurring intra-DOL, inter-DOL, and in solution respectively. Overall, the interaction process is a trimolecular reaction where Aⁱ or Bⁱ intermediate is formed first as a bimolecular reversible process between a receptor and a reporter molecule (Supplementary Figure 2). Either intermediate can interact irreversibly with another complementary active receptor to form a ternary complex for which the rate constant was derived from a reaction between reporter complex and non-cholesterol-modified receptors in solution (Fig. 2f, note the receptor concentration is approximately two orders of magnitude higher than DOL cases in order to observe faster saturation kinetics; contrasting gray curve in Fig. 3b with receptors at 5 nM). Receptor complexes were made with linker and anchor strands without cholesterol modifications

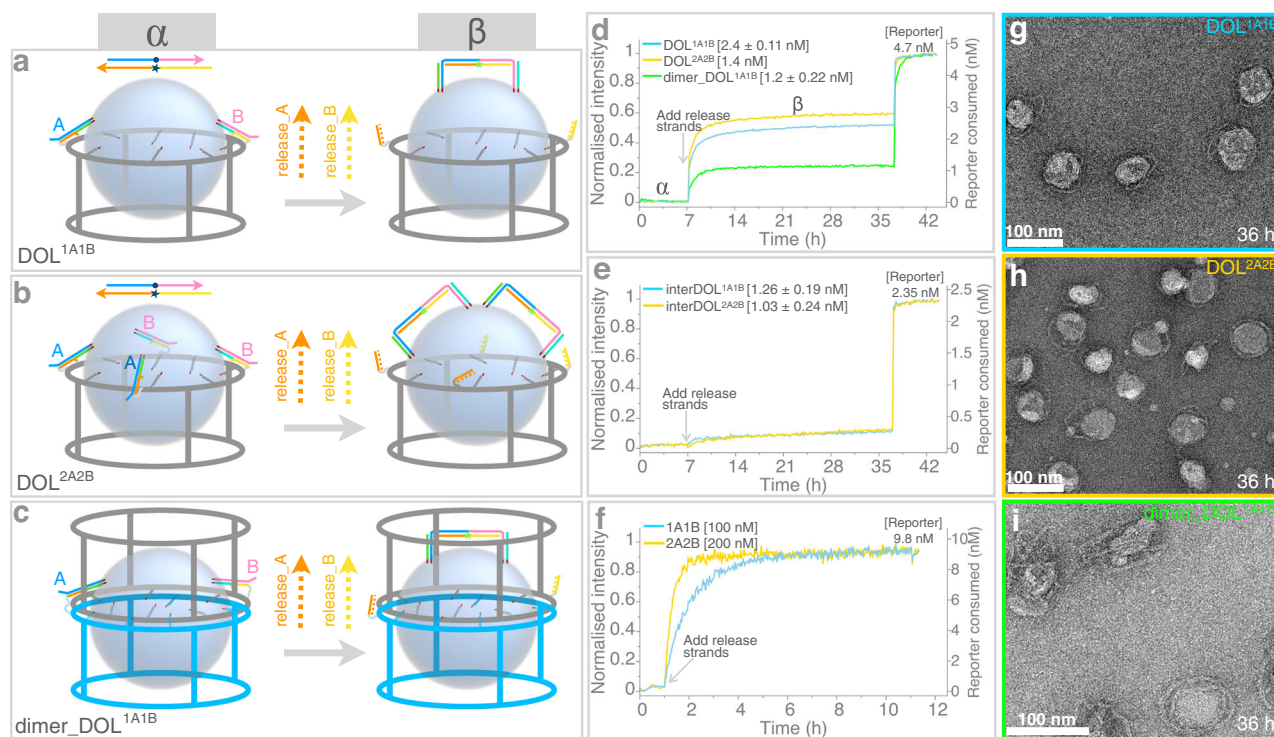


Fig. 2 | Receptor reactions on three DOL variants. **a–c** Different platforms studied by varying the number of receptors or rings. Right side of arrow shows the ternary complex depending on the initial number of receptors tethered on a DOL platform (left side of arrow). The DNA circuit logic (Fig. 1b) is same in **a–c**. Labels α and β represent the states corresponding to fluorescence intensity curves in **d**. **d** Kinetics curves acquired from plate reader experiments shown for receptor interaction event on the same surface of DOL (intra-DOL): DOL^{1A1B} (cyan curve, pooled fraction 3 + 4, two repeats averaged), DOL^{2A2B} (orange curve, fraction 5, single repeat), and dimer_DOL^{1A1B} (green curve, fraction 6, two repeats averaged). Initial 7 h has DOL with reporter complex (4.7 nM). After 7 h release strands (100 nM) were added. DOL concentrations are the saturation endpoints, with single standard deviation (in square brackets) for two repeats where performed. Unreacted reporter was unquenched by adding excess of stimulant strands at 36 h evident as a quick spike in fluorescence. **e** Kinetics curves shown for receptor

interaction between two different DOLs (inter-DOL) each containing only one receptor type: interDOL^{1A1B} and interDOL^{2A2B}. In all cases pooled fraction 3 + 4 were used and two repeats were performed (averaged curves shown). Concentrations were estimated from TEM data (see Supplementary Note 4). **f** Kinetics curves (averaged, three repeats each) shown for receptor interaction in solution. Receptors were activated by adding release strands. Plate reader experiment details in **e** and **f** are similar to **d**. Supplementary Figure 3 shows standard deviations for **d–f**. **g–i** TEM images for the samples taken after completion of plate reader experiment (after 36 h) for the DOL cases in **d**. Similar TEM images observed in three different experiments for **g** and **h** and two different experiments for **i**. TEM images for inter-DOL cases in **e** are shown in Supplementary Figure 9. DOL; DNA origami liposome, 1A/2A; one or two Receptor_A; 1B/2B, one or two Receptor_B. Specific role of DNA domains shown in different colors in **a** explained in Supplementary Table 1. **d–f** data provided as a Source Data file.

(Receptor_A consists of linker_A, anchor_A* and anchor_A, and similar for Receptor_B). Using similar plate reader experiments, as for the DOL cases, the receptors were activated by adding release strands. For 1A1B case each receptor type was at 100 nM with release strands at 900 nM and for 2A2B case these were at 200 nM and 1800 nM respectively, reporter complex was at 9.8 nM for both cases. Adding excess of stimulant strands did not show any further spike in fluorescence as all of the reporter molecules were consumed by receptors already in excess. Using the model described in Supplementary Note 6 and Supplementary Figure 10, we deduce that, due to high local receptor concentration and constraints on a fluid surface, the effective rate constant of reaction is 2800-fold higher in DOL-bound receptors than that measured in the solution case. Our model fits very well considering 1A1B and 2A2B stoichiometries used in our DOL-based experiments.

Receptor tethering efficiency

Absolute stoichiometry control requires nearly 100% tethering efficiency of receptors. The DNA logic gate used for our DOL platforms is cooperative, requiring two different receptor types to react with the reporter. If the tethering of receptors on the DOL ring is not 100% efficient, then it is possible to have four different DOL populations in the same purified fraction: DOL with no receptors, DOL with only

Receptor_A, DOL with only Receptor_B, and DOL with both the receptors.

To evaluate tethering efficiency in DOL^{1A1B}, we implement a DNA logic as shown in Fig. 3a. The logic is similar to the logic shown in Fig. 1b, but in this case, only one receptor from DOL^{1A1B} platform was released while the other receptor remained tethered to the DNA scaffold. For example, the starting reaction mixture contained reporter complex (14 nM final concentration) with the purified DOL^{1A1B} along with an excess of stimulant strand (200 nM final concentration, a non-cholesterol version of anchor_B). The stimulant strand only partially triggers the reporter complex which does not completely displace the BHQ top strand. No rise in fluorescence was observed for the first 7 h (Fig. 3b, red curve). After this, release_A (final concentration 200 nM) was added to selectively release Receptor_A which resulted in a sharp rise in fluorescence (red curve). A similar procedure was adopted to selectively release Receptor_B (blue curve), or both receptors at the same time (cyan curve).

Individually, completion levels of both the receptors, measured as a fraction of the total reporter complex consumed after all reporter is triggered, are about the same: -4.9 nM for Receptor_A and -4.7 nM for Receptor_B. This indicates that the tethering efficiency is similar for both receptors. The concentration of DOLs with both receptors active is -4.1 nM (completion level). Further, total concentration of DOL (containing both the receptors and assuming at least one receptor on

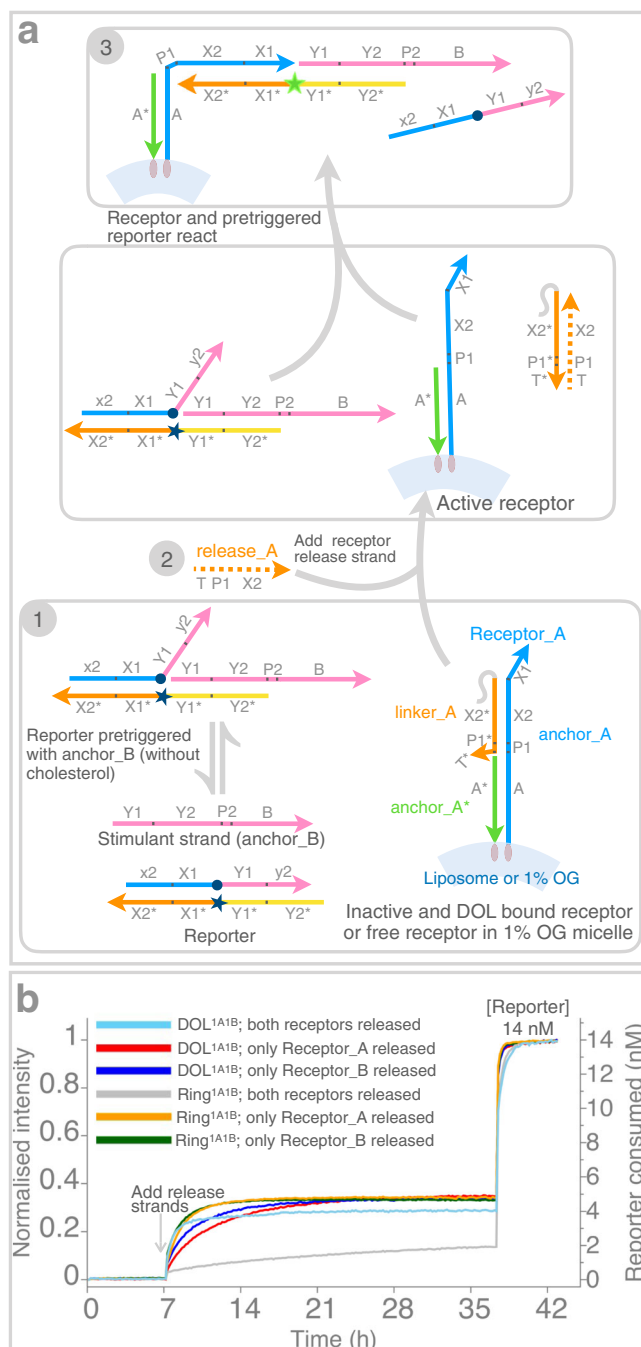


Fig. 3 | Determining tethering efficiency. Tethering efficiency of receptors to the DOL^{1A1B} platform was determined by comparing the extent of receptor reaction when one or both the receptors were released and reacted normally within the DOL, and when one or both the receptors reacted with a receptor complex in the presence of a stimulant strand in solution. **a** shows a modified logic circuit in which only receptor Receptor_A was released; a stimulant strand (anchor_B without a cholesterol modification) was supplied in excess to make up for any missing Receptor_B. A reciprocal experiment using anchor_A without a cholesterol modification is not shown. **b** Fluorescence curves (as in Fig. 2) where either both the receptors were released with a normal reporter complex (cyan), only Receptor_A

was released (red), or only Receptor_B was released (blue). Analogous curves are shown for a ring-only system (without a liposome), in which both the receptors were released (gray), only Receptor_A was released (orange, two repeats averaged), or only Receptor_B was released (green, two repeats averaged). As in Fig. 2, reporter complexes were quenched after ~36 hours with an excess of both stimulant strands, or whichever was missing. Supplementary Figure 3 shows standard deviations for Ring^{1A1B} cases. DOL; DNA origami liposome, OG; n-octyl- β -D-glucoside. DNA domains shown in different colors in **a** have a specific role as explained in Supplementary Table 1. Source data for **b** provided as a Source Data file.

each DOL is calculated to be ~5.5 nM. Thus, the calculated single labeling efficiency is ~85–89% and the double labeling efficiency is ~74%.

We also show an example where both receptors were tethered on a ring (5 nM, determined by absorption at 260 nm) without a liposome and were released together in solution (Fig. 3b, gray curve) containing

1% n-octyl- β -D-glucoside (OG) detergent. The slower kinetics, in contrast to cases where at least one stimulant strand is in excess (orange and green curves), is expected because here both the receptors are at only ~5 nM concentration. Interestingly, the saturation reached ~5 nM (almost same as ring concentration) in both cases when either of the receptors was released. This could happen in a scenario

where almost all the rings in the system have both receptors, indicating high efficiency for the liposome-free system.

Comparing the cases (gray *vs* cyan curves, Fig. 3b) when both the receptors are released from Ring^{1A1B} (no templated liposome) and DOL^{1A1B} systems, faster kinetics is observed in the later case. In Ring^{1A1B} case the receptors when released react with the reporter in the bulk solution and the overall kinetics is rate limited by their diffusion. Whereas in DOL^{1A1B} case the reaction kinetics is faster because the receptors are released and co-localized on the same lipid surface (high local concentration).

Discussion

Here we have shown stoichiometric, spatial, and temporal (S²T) control for DNA receptor complexes in membranes for two different stoichiometries, which in principle could be scaled to different stoichiometries. A number of previous studies have examined the reaction of DNA receptors in membranes, either for the purpose of creating DNA circuits^{48–51}, studying diffusion within bilayers⁷⁰, or creating artificial signaling systems capable of transducing a DNA receptor dimerization event across a membrane^{71,72}. In particular, one study⁴⁹ showed mild (75%) rate acceleration and significantly decreased leak for TMSD receptor reactions confined to liposomes, in the context of uncontrolled absolute stoichiometry. While none of these DNA receptor systems have achieved full S²T control, they provide inspiration for future uses of DOL. In the case of circuits, DOL will enable the implementation of systems where exact numbers of molecular inputs are required, or where each DNA computation cannot tolerate cross-talk with other copies of the DNA computation and must run within its own self-contained volume⁷³. And while we have demonstrated the release of up to four receptor reactants into the membrane, staple extensions on our current DOL could easily support the independently triggered release of several dozen different inputs, as required by a circuit, signaling cascade, or investigation of a biological question.

In our current approach, the receptors' active domains (for release strand and reporter binding) are positioned between the linker to the ring and the hydrophobic groups (cholesterols) used as membrane anchors. This ensures that active domains are positioned outside of the liposome. On the other hand, signalling transduction systems^{71,72} suggest that it will be important to control the orientation of receptors inserted into DOL membranes, so that signal output domains can be positioned within the lumen of the DOL–intra-liposomally—when desired. In our system, an intraliposomal domain could be added by (1) lengthening the hydrophobic groups so that they become a transmembrane domain and (2) attaching the desired domain to the distal end of the hydrophobic groups, so that it extends into the liposomal lumen. Ligands or auxiliary molecules meant to interact with intraliposomal domains could be either explicitly positioned with the same strategy, or simply encapsulated during the liposome formation. Where DOLs are used for membrane proteins, the position of the DNA linker (whether it is attached to the cytosolic or extracellular domain) will determine the orientation of the protein in the bilayer. When the linker is attached to the extracellular domain, the membrane protein is expected to be oriented normally so that the cytosolic domain is intraliposomal. When attached to the cytosolic domain the membrane protein will be flipped, with the cytosolic domain on the outside, where it can be studied and manipulated.

The digital nature of DOL is clearly established with: (a) a case with only one Receptor_A and one Receptor_B on DOL^{1A1B} platform (Fig. 2d), (b) another case with two Receptor_A and two Receptor_B on DOL^{2A2B} (Fig. 2d) where the fluorescence observed corresponds to 2x the concentration of the DOL platform and, coupled with point 'a', indicates 2x stoichiometry of the receptors, and (c) the tethering efficiency experiments (Fig. 3) conducted on DOL^{1A1B}, where selectively only one type of receptor is released, clearly demonstrates that there is only 1A

and only 1B on each platform. Furthermore the inter-DOL experiments (Fig. 2e) clearly show that the cross-talk (inter-DOL interactions) between the platforms is rare and most of the receptor interactions occur on the same platform (intra-DOL). This explains the nanoreactor nature of DOL. If the reaction was not localized on the DOL then one would not expect to see any difference between intra-DOL and inter-DOL cases. Thus, each DOL is essentially a well-isolated reaction vessel with a controlled copy number of reactants—a digital nanoreactor. A bulk sample of DOL can therefore be measured without significant cross-reactions between vessels. As a result, properties which have until now required sophisticated single-molecule (or single liposome) techniques, can be measured using DOL via bulk fluorescence in a common plate reader. Detailed variation between reaction trajectories on different liposomes is, of course, averaged out by such bulk measurements, but variability in the number of molecules that can participate in a reaction is tightly controlled. In contrast, depending on the specific reactants and their concentrations, the extent of oligomerization and resulting size of aggregates can be unlimited in-bulk experiments. As we have shown, bulk measurement of kinetics on DOL provides a sort of integration over digital nanoreactors that preserves kinetics as a function of copy number and maintains confinement of reactants to the restricted environment of the nanoreactor. Thus, while DOL could be examined with a single-molecule technique, the DOL platform also enables a type of experiment whose window on the molecular world lies somewhere between that of a single-molecule experiment and classical bulk technique (single molecule in-bulk assay).

We note that DNA nanostructure^{74,75}, DNA micelle⁷⁶, protein organelle⁷⁷, protein nanopore⁷⁸, viral⁷⁹, vesicle⁸⁰, MOFs⁸¹, and polymersome⁸² nanoreactors or zeptoreactors⁸³ have been explored before, but none with the specific advantages provided by DOL. Viral capsids have encapsulated single enzymes⁷⁹ and hollow DNA origami have encapsulated exact numbers of enzymes within a cascade^{84,85} but neither has yet enabled the exact number of reactants to be defined. DNA origami with reactants constrained to remain on their surface^{34–38} provide fully digital nanoreactors, with total control over the type and number of all reactants. Such membrane-free platforms have even stronger spatial control than do DOL, able to control local geometric configuration and reaction sequence. Especially interesting for applications in signal amplification³⁷, DNA computing³⁸ and molecular robotics^{34–36}, they purchase extra spatial control at the cost of preventing reactants from diffusing freely within the nanoreactor, as occurs in our DOL platform.

With respect to diffusion of reactants within the DOL, several questions remain. Here we have not verified that the effective reaction area of the nanoreactors scales linearly with the membrane area of the liposome (e.g., by making larger or smaller liposomes). We have similarly not verified that receptors positioned away from the equator of the ring (say at opposite poles) exhibit similar behavior to those immobilized at the equator, to demonstrate the free diffusion of receptors from one hemisphere to the other (across the liposome's zone of contact with the ring). Experiments to verify these aspects of DOL will be required to delineate the conditions under which DOL can be modeled as simple nanoreactors in which the membrane is homogeneous and its biophysical properties (e.g., receptor diffusion constant) are independent of DOL size. For proteins whose oligomerization behavior depends on membrane curvature^{86,87}, the assumption of DOL size-independent behavior will likely fail, making modeling more challenging. On the positive side, wherever membrane biophysics does turn out to be DOL size-dependent, development of a series of DOL having a range of diameters could enable new opportunities—e.g., protein sensors of membrane curvature could be studied and engineered. Furthermore, it would be interesting to test how different lipid compositions can effectively change the receptor diffusion rates which can potentially impact reaction kinetics or to localize

different receptors in biologically relevant phase-separated regions as cell membrane synthetic mimics^{52,88,89}. Most of such studies are conducted using giant vesicles in μm range, which can be characterized using confocal microscopy. Characterization could be challenging for our templated liposomes which are in nanometer scale ($\sim 45\text{ nm}$) and other methodologies would need to be adopted.

Because the main motivation of this work is the eventual study and control of membrane protein interactions, it is important to discuss both the prospects and potential challenges. In principle, DOL platform could be used for membrane protein interactions by replacing the DNA receptors with DNA-conjugated membrane proteins, where the protein-DNA linkers carry appropriate FRET probes. DOL are currently hybridized with cholesterol-modified DNA receptors in the presence of detergent, and so tethering detergent-solubilized membrane proteins (conjugated to appropriate DNA linkers) under similar conditions should be possible. However, as currently cast, the DOL system best models ligand or chemically induced protein interactions, where the reporter complex acts as the ligand to mediate receptor interactions. Such mediation by the reporter complex, as well as triggered activation of the receptor toeholds for the reporter complex by the release strands, provide two levels of protection against any receptor interaction before it is desired. The result is that the DOL is resistant against receptor-mediated inter-DOL leak reactions and DOL aggregation. In the case of ligand-induced protein interactions, where the proteins under study should have weak interactions before the introduction of the appropriate ligand, we expect that the current DOL will perform adequately.

In the case of proteins with constitutive interactions⁹⁰ new techniques will be required to use DOL with minimal leak and aggregation; that is to keep proteins in their monomeric states. One approach may be to disrupt salt-sensitive constitutive interactions with high salt during synthesis and purification, before performing a concomitant trigger and buffer exchange step. Depending on the speed of intra-DOL versus inter-DOL reactions, this approach may be sufficient. For some proteins, whose interactions are denatured by detergent before the liposome-forming step removes the detergent, orienting their oligomerization domains to the inside of the lumen may be sufficient. A more general and robust solution would be to use DNA scaffold geometry to prevent inter-DOL protein interaction. In principle, this could be achieved by an extension of the dimer-DOL synthetic approach that we have already demonstrated. Instead of attaching proteins to open ring-like origami, any proteins with constitutive interactions could be hidden inside a pair of DNA origami barrels⁹¹, prepared in separate test tubes. End-to-end heterodimerization of the barrels would result in a dimer-DOL with no propensity to aggregate, and a liposome could be assembled inside so that it filled the interior of both barrels⁹¹ and embedded both membrane proteins. For multi-protein interactions, such a steric protection strategy could be extended to as many barrels as necessary, as extended liposomes have been created by filling chains of more than ten concatenated origami scaffolds⁹¹.

Lastly, there may be situations wherein the DNA linkers to a protein interfere with protein-protein interactions. In this case, TMSD release mechanisms could be replaced with photocleavable groups⁹², which would free proteins from their DNA linkers at the time of release. Overall, with some extensions to the basic technique, DOL digital nanoreactors may have the potential to provide custom instruments for the study and dissection of even the most complex membrane protein interactions.

Methods

Materials

Modified and unmodified DNA strands were purchased from Integrated DNA Technologies (IDT, USA). All staple strands, except those with linker extensions, were obtained and used in an unpurified form.

Staples with linker_A or linker_B extensions were either purchased HPLC-purified or purchased unpurified and PAGE-purified in-house before use. All receptor and reporter complex strands were purchased HPLC-purified, dissolved in $1\times$ TE buffer, and stored at -20°C . Sequences for cholesterol-modified DNA (with a triethylene glycol linker), including IDT modification codes are provided in Supplementary Table 1. Lipids were purchased from Avanti Polar Lipids, USA. Gels were imaged using a ChemiDoc MP instrument (Biorad, USA). Catalog numbers for the chemicals used in this study are provided as Supplementary Data 1. In many buffers n-octyl- β -D-glucoside (OG) was added as a detergent. Origami annealing buffer is $1\times$ TE, 12.5 mM MgCl_2 ; TE-Mg buffer is $1\times$ TE, 10 mM MgCl_2 ; TAE-Mg buffer is $1\times$ TAE, 10 mM MgCl_2 ; TE-Mg-OG buffer is 1% OG, $1\times$ TE, 10 mM MgCl_2 ; HEPES-Mg-K is 10 mM MgCl_2 , 25 mM HEPES , 100 mM KCl ; HEPES-OG buffer is 1% OG in HEPES-Mg-K; in all cases 25 mM HEPES buffer pH 7.4 adjusted with KOH. Where possible, final concentrations (f.c.) of solution components are given.

Ring design, assembly, and purification

We used a DNA origami ring design reported earlier⁵⁹ with slight modifications for positioning linker strands. cadNano⁹³ design is provided as Supplementary Software file (see cadnano) and DNA staple sequences are provided as Supplementary Data 2. DNA scaffold strand (8,064 nucleotide) was produced from *E. coli* and M13-derived bacteriophages²⁹. *E. coli* K91endA cells were cultured in YT medium supplemented with 5 mM MgCl_2 at 37°C . When OD₆₀₀ reached 0.4, the bacteria were transformed with p8064 phage, and continued growing at 37°C for 4 h. Bacterial cells were then pelleted by centrifugation and ssDNA phages were recovered from the supernatant by PEG precipitation (4% PEG8000, 0.5 M NaCl). After resuspension in 25 mM Tris (pH 8.0) and purification by centrifugation, p8064 scaffold was isolated from phage by alkaline/detergent denaturation (2 volume of 0.2 M NaOH and 1% SDS, followed by 1.5 volume of 3 M KOAc) and ethanol precipitation. Final ssDNA product was resuspended in 10 mM Tris (pH 8.0) and its concentration was determined by Nanodrop. DNA scaffold (8,064 nucleotide), 100 nM f.c. , was mixed with $6\times$ excess of staple strands, including linker strands in origami annealing buffer. Typically, $1000\ \mu\text{L}$ reaction mix (scaffold and staples) was prepared and divided in 20 tubes. All tubes were annealed from 95 to 20°C over 36 h and then the annealed reactions were pooled and concentrated using 30 kDa Amicon 0.5 mL centrifugal filters. Filters were pre-wetted with TE-Mg by centrifuging at $6000\times g$ for 4 minutes. Afterward, pooled annealed reaction mix was concentrated by loading $500\ \mu\text{L}$ volume in two different filters by centrifuging at 8000 rpm for 8 minutes. The concentrated sample (total $\sim 180\ \mu\text{L}$) was mixed with glycerol (f.c. $\sim 7\%$) and divided in two equal volumes for further purification. To make a gradient, $\sim 2.5\text{ mL}$ each of 15 and 45% glycerol in TE-Mg were loaded initially into an ultracentrifuge tube to form two layers, which were converted into a continuous gradient using Biocomp gradient station. Finally, each volume (in 7% glycerol mentioned above) was loaded on top of freshly made gradient and purified using rate-zonal ultracentrifugation by rotating at $304,000\times g$ for 1 h at 4°C . After this, ~ 20 fractions ($200\ \mu\text{L}$ each) were collected manually from the centrifuge tubes. To determine the fraction containing desired product, $5\ \mu\text{L}$ of each fraction was loaded in 1.5% agarose gel (prepared with TAE-Mg buffer having ethidium bromide as a pre-stain) and the gel was run at room temperature by applying 60 V for 1.5 h in TAE-Mg. Based on gel results (Supplementary Figure 1b) the desired fractions were pooled and concentrated using 30 kDa Amicon 0.5 mL centrifugal filters (as above). At the end of this step, only trace amounts of staples remained. To remove glycerol from the concentrated sample, we performed one or two $400\ \mu\text{L}$ TE-Mg washes; trace glycerol at this step did not affect downstream steps. Ring concentration was measured by UV absorption at 260 nm using a Nanodrop

spectrophotometer. Purified rings were stored at 4 °C (and used within a week) or -20 °C (and used within 1 or 2 months).

Annealing reporter and receptors

For the reporter complex, top strand (with black hole quencher, see Table 1 for IDT order code) was added in 1.5× excess of the bottom strand (with fluorescein, see Table 1 for IDT code) with f.c. 300 nM and 200 nM respectively. The total volume in TE-Mg buffer was ~1000 μL. Reaction mix was annealed in different tubes (each ~100 μL) from 95 to 20 °C over 2 h. Annealed reactions were pooled together, stored at 4 °C, and later used without further purification. The same batch of reporter complex was used for all plate reader measurements. Freshly thawed and annealed volumes of cholesterol receptor complexes were used for each experiment. 10 μM aliquots of the cholesterol-modified strands stored at -20 °C were thawed at room temperature at least for 1 h. Annealing was performed from 95 to 20 °C over 2 h using 2× excess of anchor_A* or anchor_B* (f.c. 600 nM) with anchor_A or anchor_B (f.c. 300 nM) in TE-Mg-OG. Annealed receptors were used further without purification.

Tethering DNA receptors to rings and purification

Purified rings containing linkers were incubated with freshly annealed receptors at 37 °C for 1 h in TE-Mg-OG buffer modified to have 1.15× OG. For DOL^{IAIB}, Receptor_A and Receptor_B (f.c. 90 nM each) were added at 3× in excess of ring (f.c. 30 nM) containing one linker_A and one linker_B. For DOL^{2A2B}, Receptor_A and Receptor_B (f.c. 135 nM each) were 4.5× in excess of ring (f.c. 30 nM) containing two linker_A and two linker_B. In general, the total incubation volume was ~200 μL. To remove the excess receptors and to determine the desired fractions, we followed a rate-zonal ultracentrifugation purification procedure and agarose gel analysis steps similar to those described above for rings, with minor differences. Here, a 15–45% glycerol gradient was prepared with detergent (in TE-Mg-OG) and centrifuged at 10 °C (rather than 4 °C). Desired fractions were pooled and concentrated using 30 kDa 0.5 mL Amicon centrifugal filters, with one or two 400 μL final TE-Mg-OG buffer washes. Ring concentration was estimated by UV absorption at 260 nm using a Nanodrop spectrophotometer; the purified product was stored at 4 °C and used the next day.

DOL formation and purification

Stock 10 mM lipid mixture was made with 75:20:5 molar ratio of 1,2-dioleoyl-sn-glycero-3-phosphocholine (DOPC), 1,2-dioleoyl-sn-glycero-3-phospho-L-serine (DOPS), 1,2-dioleoyl-sn-glycero-3-phosphoethanolamine-N-[methoxy(polyethylene glycol)-2000] (PEG2000-PE) respectively in chloroform (f.c.: 7.5 mM DOPC, 2 mM DOPS, 0.5 mM PEG2000-PE). A desired volume of this stock was dried under nitrogen gas for 10–20 min and then further dried for 3 h in a freeze dryer (Freezone 1, Labconco). For use, dried lipids were rehydrated to a concentration of 10 mM lipids with 25 mM HEPES and 100 mM KCl buffer and shaken for 0.5 h at room temperature. The ring has handles (32 staple extensions in the case of two receptors and 30 for four receptors), which can hybridize with anti-handles made of cholesterol-modified oligonucleotides (Step C, Fig. 1a). These anti-handles act as seeds for liposome formation. Each purified sample of 'rings with hybridized receptors' (f.c. 30 nM) was incubated with cholesterol-containing antihandles (f.c. 1.8 μM) at 37 °C for 1 h in HEPES-OG buffer. After incubation, each sample of 'rings with hybridized receptors and anti-handles' (f.c. 15 nM) was mixed with hydrated lipids (f.c. 1.5 mM) in HEPES-OG buffer to create a total volume ~150 μL and was shaken gently for 0.5 h at 25 °C. To remove the detergent and to form liposomes inside the rings, the mixture was transferred to Slide-A-Lyzer 0.5 mL 7 kDa dialysis cassette using a syringe. Dialysis was done overnight at room temperature against 2 L HEPES-OG buffer.

To purify the dialysis mix we performed isopycnic ultracentrifugation, using 6–30% iodixanol gradients in HEPES-Mg-K where

less dense free liposomes float to the top, and rings holding liposomes are distributed in lower fractions. After overnight dialysis we typically recovered ~210 μL per sample. For each sample, 200 μL was used and divided in two 100 μL replicates and each replicate was mixed with 200 μL of 45% iodixanol in HEPES-Mg-K. Thus for each replicate a total of 300 μL containing 30% iodixanol was placed at the bottom of an ultracentrifuge tube, above which 60 μL each of 26%, 22%, 18%, 14%, 10%, and 6% of iodixanol were layered (bottom to top) via manual pipetting. Samples were centrifuged at 280,000 × *g* for 5 h at 4 °C and twelve or thirteen 50 μL fractions were collected from each centrifuge tube. Fractions were collected in tubes that had been pre-rinsed with a blocking solution (1 μM 15 T oligonucleotides in HEPES-Mg-K buffer); all tubes used after this step (for pooling or transfer) are also pre-rinsed with blocking solution. For each DOL, identical fractions from replicates were pooled, and pooled fraction 3 and fraction 4 were further combined. To each pooled sample 15 T oligo was added to 1 μM f.c.

Fluorescence plate reader experiments

Biotek Cytation-1 plate reader was used for real-time fluorescence measurements. Plate reader measurements were done at 25 °C using a 475/20 nm excitation filter and a 530/25 nm emission filter. Samples were loaded manually into Corning 384-well assay plates (black with clear flat bottoms). To avoid sample evaporation, plate wells were sealed with Nunc polyolefin acrylate sealing tape. Before loading samples, wells were pipette-rinsed with blocking solution. To each DOL tested, reporter complex was added (4.7 or 14 nM f.c.) and samples were mixed gently via manual pipetting. Next, 46.2 μL of each sample was loaded per well, making sure no air bubbles were trapped in the wells. Baseline fluorescence was first measured for ~7 h. Release strands were added (0.9 μL of a stock containing 5 μM each of release_A and release_B to create ~100 nM f.c. of each release strand) to initiate receptor interactions, which were measured for a further ~18 h. To establish a maximum fluorescence endpoint, with which each sample trace could be normalized, we triggered any remaining reporter complex by adding excess anchor_A and anchor_B strands (versions without cholesterol modifications, to 100 nM f.c. for each) and then measured the fluorescence for another 4 to 6 h. Data files for kinetics curves are provided as Source Data. PERL scripts for data analyses and chemical reaction networks (CRN) simulator are provided as Supplementary Software files (see crn and perl_scripts folders and corresponding Readme files).

TEM sample preparation

Uranyl formate negative-stain solution (1% w/v) is acidic and can denature DNA nanostructures; thus 1 mL aliquots were neutralized by adding 2.5 μL of 5 M NaOH prior to use (see guidelines for preparation and storage elsewhere⁹⁴). DOL samples (5 μL) were deposited on a glow-discharged formvar/carbon-coated copper grid (Ted Pella, Inc.) for 1 minute, and the liquid was blotted away using filter paper. Each grid was subsequently washed with 7.5 μL of HEPES-Mg-K buffer and stained with 7.5 μL neutralized uranyl formate negative-stain for 1 minute. Negative-stain TEM images were acquired using an FEI Tecnai T12 TEM (120 kV) equipped with an EDS detector and 4k x 4k Gatan Ultrascan CCD.

Analyses and plots

Raw plate reader data (in text format) analyses were performed using custom PERL v5.16.3 scripts. Plots were created using XMGRACE Grace-5.1⁹⁵ or gnuplot v5.4 (www.gnuplot.info). CRNSimulator (<http://users.ece.utexas.edu/~soloveichik/crn simulator.html>) was used for reaction simulations.

Statistics and reproducibility

No sample-size calculation was performed. Experiments were repeated 2–3 times on different occasions (different day, different starting

sample) with 2–3 copies for many samples on each occasion. Data are reproducible in this in vitro setup, and results from different experiments corroborate each other. Plate reader well positions were chosen randomly and data were normalized with respect to each well independently (baseline fluorescence subtracted). The person who performed TEM imaging was blinded to the sample identities.

Reporting summary

Further information on research design is available in the Nature Portfolio Reporting Summary linked to this article.

Data availability

Data in Figs. 2 and 3, Supplementary Figures 3–6, 8, and 10, and DNA receptor sequences in Table 1 and Supplementary Table 1 are provided in the Source Data file. Chemicals catalogs are provided as Supplementary Data 1 and DNA staple sequences are provided as Supplementary Data 2. Source data are provided with this paper.

Code availability

Files related to DNA origami design (see folder cadnano), CRN simulator (see folder crn), and PERL scripts (see folder perl_scripts) are provided as Supplementary Software files.

References

1. Cho, W. & Stahelin, R. V. Membrane-protein interactions in cell signaling and membrane trafficking. *Annu. Rev. Biophys. Biomol. Struct.* **34**, 119–151 (2005).
2. Khoubza, L., Chatelain, F. C., Feliciangeli, S., Lesage, F. & Bichet, D. Physiological roles of heteromerization: focus on the two-pore domain potassium channels. *J. Physiol.* **599**, 1041–1055 (2021).
3. Kasai, R. S. & Kusumi, A. Single-molecule imaging revealed dynamic GPCR dimerization. *Curr. Opin. Cell Biol.* **27**, 78–86 (2014).
4. Milligan, G., Ward, R. J. & Marsango, S. GPCR homo-oligomerization. *Curr. Opin. Cell Biol.* **57**, 40–47 (2019).
5. Singh, D. R., King, C., Salotto, M. & Hristova, K. Revisiting a controversy: the effect of EGF on EGFR dimer stability. *Biochim. Biophys. Acta Biomembr.* **1862**, 183015 (2020).
6. George, S. R., O'Dowd, B. F. & Lee, S. P. G-protein-coupled receptor oligomerization and its potential for drug discovery. *Nat. Rev. Drug Discov.* **1**, 808–820 (2002).
7. Yin, H. & Flynn, A. D. Drugging membrane protein interactions. *Annu. Rev. Biomed. Eng.* **18**, 51–76 (2016).
8. Tsigelny, I. F. et al. Mechanisms of hybrid oligomer formation in the pathogenesis of combined Alzheimer's and Parkinson's diseases. *PLoS One* **3**, e3135 (2008).
9. Bagheri, Y., Ali, A. A. & You, M. Current methods for detecting cell membrane transient interactions. *Front. Chem.* **8**, 1074 (2020).
10. Watt, A. D. et al. Oligomers, fact or artefact? SDS-PAGE induces dimerization of β -amyloid in human brain samples. *Acta Neuropathol.* **125**, 549–564 (2013).
11. Weerasekera, R. & Schmitt-Ulms, G. Crosslinking strategies for the study of membrane protein complexes and protein interaction interfaces. *Biotechnol. Genet. Eng. Rev.* **23**, 41–62 (2006).
12. Sasmal, D. K., Pulido, L. E., Kasal, S. & Huang, J. Single-molecule fluorescence resonance energy transfer in molecular biology. *Nanoscale* **8**, 19928–19944 (2016).
13. Stockbridge, R. B., Robertson, J. L., Kolmakova-Partensky, L. & Miller, C. A family of fluoride-specific ion channels with dual-topology architecture. *Elife* **2**, e01084 (2013).
14. Chadda, R. & Robertson, J. L. Chapter three - measuring membrane protein dimerization equilibrium in lipid bilayers by single-molecule fluorescence microscopy. In *Single-Molecule Enzymology: Fluorescence-Based and High-Throughput Methods*; Spies, M., Chemla, Y. R. B. T.-M. in E., Eds., Vol. 581, pp 53–82 (Academic Press, 2016).
15. King, C., Raicu, V. & Hristova, K. Understanding the FRET signatures of interacting membrane proteins. *J. Biol. Chem.* **292**, 5291–5310 (2017).
16. Wang, Y. et al. Single molecule FRET reveals pore size and opening mechanism of a mechano-sensitive ion channel. *Elife* **3**, e01834 (2014).
17. Gupta, K. et al. The role of interfacial lipids in stabilizing membrane protein oligomers. *Nature* **541**, 421–424 (2017).
18. Funke, J. J. et al. Uncovering the forces between nucleosomes using DNA origami. *Sci. Adv.* **2**, e1600974 (2016).
19. Shaw, A. et al. Binding to nanopatterned antigens is dominated by the spatial tolerance of antibodies. *Nat. Nanotechnol.* **14**, 184–190 (2019).
20. Dong, R. et al. DNA origami patterning of synthetic T cell receptors reveals spatial control of the sensitivity and kinetics of signal activation. *Proc. Natl Acad. Sci.* **118**, e2109057118 (2021).
21. Aksel, T., Yu, Z., Cheng, Y. & Douglas, S. M. Molecular goniometers for single-particle cryo-electron microscopy of DNA-binding proteins. *Nat. Biotechnol.* **39**, 378–386 (2021).
22. Endo, M. et al. Single-molecule manipulation of the duplex formation and dissociation at the G-quadruplex/i-motif site in the DNA nanostructure. *ACS Nano* **9**, 9922–9929 (2015).
23. Suzuki, Y. et al. DNA origami based visualization system for studying site-specific recombination events. *J. Am. Chem. Soc.* **136**, 211–218 (2014).
24. Kosuri, P., Altheimer, B. D., Dai, M., Yin, P. & Zhuang, X. Rotation tracking of genome-processing enzymes using DNA origami rotors. *Nature* **572**, 136–140 (2019).
25. Cai, X. et al. DNA nunchucks: nanoinstrumentation for single-molecule measurement of stiffness and bending. *Nano Lett.* **20**, 1388–1395 (2020).
26. Dey, S. et al. DNA origami. *Nat. Rev. Methods Prim.* **1**, 13 (2021).
27. Rothmund, P. W. K. Folding DNA to create nanoscale shapes and patterns. *Nature* **440**, 297–302 (2006).
28. Wei, B., Dai, M. & Yin, P. Complex shapes self-assembled from single-stranded DNA tiles. *Nature* **485**, 623–626 (2012).
29. Douglas, S. M. et al. Self-assembly of DNA into nanoscale three-dimensional shapes. *Nature* **459**, 414–418 (2009).
30. Ke, Y., Ong, L. L., Shih, W. M. & Yin, P. Three-dimensional structures self-assembled from DNA bricks. *Science* **338**, 1177–1183 (2012).
31. Ramezani, H. & Dietz, H. Building machines with DNA molecules. *Nat. Rev. Genet.* **21**, 5–26 (2020).
32. Chandrasekaran, A. R. Programmable DNA scaffolds for spatially-ordered protein assembly. *Nanoscale* **8**, 4436–4446 (2016).
33. Hannewald, N. et al. DNA origami meets polymers: a powerful tool for the design of defined nanostructures. *Angew. Chem. Int. Ed.* **60**, 6218–6229 (2021).
34. Lund, K. et al. Molecular robots guided by prescriptive landscapes. *Nature* **465**, 206–210 (2010).
35. Thubagere, A. J. et al. A cargo-sorting DNA robot. *Science* **357**, eaan6558 (2017).
36. Wickham, S. F. J. et al. A DNA-based molecular motor that can navigate a network of tracks. *Nat. Nanotechnol.* **7**, 169–173 (2012).
37. Bui, H. et al. Localized DNA hybridization chain reactions on DNA origami. *ACS Nano* **12**, 1146–1155 (2018).
38. Qian, L. & Winfree, E. Parallel and Scalable Computation and Spatial Dynamics with DNA-Based Chemical Reaction Networks on a Surface - DNA Computing and Molecular Programming; Murata, S., Kobayashi, S., Eds.; Springer International Publishing: Cham, 2014; pp 114–131.
39. Yang, Y. et al. Self-assembly of size-controlled liposomes on DNA nanotemplates. *Nat. Chem.* **8**, 476 (2016).

40. Darley, E., Singh, J. K. D., Surace, N. A., Wickham, S. F. J. & Baker, M. A. B. The fusion of lipid and DNA nanotechnology. *Genes (Basel)*. **10**, 1001 (2019).
41. Moggetti, B. M., Cicuta, P. & Di Michele, L. Programmable interactions with biomimetic DNA linkers at fluid membranes and interfaces. *Rep. Prog. Phys.* **82**, 116601 (2019).
42. Burns, J. R., Stulz, E. & Howorka, S. Self-assembled DNA nanopores that span lipid bilayers. *Nano Lett.* **13**, 2351–2356 (2013).
43. Langecker, M. et al. Synthetic lipid membrane channels formed by designed DNA nanostructures. *Science* **338**, 932–936 (2012).
44. Franquelim, H. G., Khmelinskaja, A., Sobczak, J.-P., Dietz, H. & Schwille, P. Membrane sculpting by curved DNA origami scaffolds. *Nat. Commun.* **9**, 811 (2018).
45. Zhao, Z. et al. DNA-corralled nanodiscs for the structural and functional characterization of membrane proteins and viral entry. *J. Am. Chem. Soc.* **140**, 10639–10643 (2018).
46. Iric, K. et al. DNA-encircled lipid bilayers. *Nanoscale* **10**, 18463–18467 (2018).
47. Zhang, Z. & Chapman, E. R. Programmable nanodisc patterning by DNA origami. *Nano Lett.* **20**, 6032–6037 (2020).
48. Fabry-Wood, A. et al. A microsphere-supported lipid bilayer platform for DNA reactions on a fluid surface. *ACS Appl. Mater. Interfaces* **9**, 30185–30195 (2017).
49. Kaufhold, W. T., Brady, R. A., Tuffnell, J. M., Cicuta, P. & Di Michele, L. Membrane scaffolds enhance the responsiveness and stability of DNA-based sensing circuits. *Bioconjug. Chem.* **30**, 1850–1859 (2019).
50. Seo, J., Kim, S., Park, H. H., Choi, D. Y. & Nam, J.-M. Nano-bio-computing lipid nanotablet. *Sci. Adv.* **5**, eaau2124 (2019).
51. Song, T. et al. Programming DNA-based biomolecular reaction networks on cancer cell membranes. *J. Am. Chem. Soc.* **141**, 16539–16543 (2019).
52. Beales, P. A. & Vanderlick, T. K. Application of nucleic acid–lipid conjugates for the programmable organisation of liposomal modules. *Adv. Colloid Interface Sci.* **207**, 290–305 (2014).
53. Lopez, A. & Liu, J. DNA oligonucleotide-functionalized liposomes: bioconjugate chemistry, biointerfaces, and applications. *Langmuir* **34**, 15000–15013 (2018).
54. Pfeiffer, I. & Höök, F. Bivalent cholesterol-based coupling of oligonucleotides to lipid membrane assemblies. *J. Am. Chem. Soc.* **126**, 10224–10225 (2004).
55. Xu, W. et al. A programmable DNA origami platform to organize SNAREs for membrane fusion. *J. Am. Chem. Soc.* **138**, 4439–4447 (2016).
56. Löffler, P. M. G. et al. A DNA-programmed liposome fusion cascade. *Angew. Chem. Int. Ed.* **56**, 13228–13231 (2017).
57. Ries, O., Löffler, P. M. G., Rabe, A., Malavan, J. J. & Vogel, S. Efficient liposome fusion mediated by lipid–nucleic acid conjugates. *Org. Biomol. Chem.* **15**, 8936–8945 (2017).
58. Göpfrich, K., Platzman, I. & Spatz, J. P. Mastering complexity: towards bottom-up construction of multifunctional eukaryotic synthetic cells. *Trends Biotechnol.* **36**, 938–951 (2018).
59. Zhang, Z., Yang, Y., Pincet, F., Llaguno, M. C. & Lin, C. Placing and shaping liposomes with reconfigurable DNA nanocages. *Nat. Chem.* **9**, 653–659 (2017).
60. Ori, A. et al. Cell type-specific nuclear pores: a case in point for context-dependent stoichiometry of molecular machines. *Mol. Syst. Biol.* **9**, 648 (2013).
61. Akhavantabib, N., Krzizike, D. D., Neumann, V. & D’Arcy, S. Stoichiometry of Rtt109 complexes with Vps75 and histones H3–H4. *Life Sci. Alliance* **3**, e202000771 (2020).
62. Rajoo, S., Vallotton, P., Onischenko, E. & Weis, K. Stoichiometry and compositional plasticity of the yeast nuclear pore complex revealed by quantitative fluorescence microscopy. *Proc. Natl Acad. Sci.* **115**, E3969–E3977 (2018).
63. Seelig, G., Soloveichik, D., Zhang, D. Y. & Winfree, E. Enzyme-free nucleic acid logic circuits. *Science* **314**, 1585 LP–1581588 (2006).
64. Zhang, D. Y. & Seelig, G. Dynamic DNA nanotechnology using strand-displacement reactions. *Nat. Chem.* **3**, 103–113 (2011).
65. Simmel, F. C., Yurke, B. & Singh, H. R. Principles and applications of nucleic acid strand displacement reactions. *Chem. Rev.* **119**, 6326–6369 (2019).
66. Dirks, R. M., Bois, J. S., Schaeffer, J. M., Winfree, E. & Pierce, N. A. Thermodynamic analysis of interacting nucleic acid strands. *SIAM Rev.* **49**, 65–88 (2007).
67. SantaLucia, J. A unified view of polymer, dumbbell, and oligonucleotide DNA nearest-neighbor thermodynamics. *Proc. Natl Acad. Sci.* **95**, 1460 LP–1461465 (1998).
68. Morzy, D. et al. Cations regulate membrane attachment and functionality of DNA nanostructures. *J. Am. Chem. Soc.* **143**, 7358–7367 (2021).
69. Zhang, D. Y. Cooperative hybridization of oligonucleotides. *J. Am. Chem. Soc.* **133**, 1077–1086 (2011).
70. Dave, N. & Liu, J. Biomimetic sensing based on chemically induced assembly of a signaling DNA aptamer on a fluid bilayer membrane. *Chem. Commun.* **48**, 3718–3720 (2012).
71. Chen, H. et al. Controlled dimerization of artificial membrane receptors for transmembrane signal transduction. *Chem. Sci.* **12**, 8224–8230 (2021).
72. Liu, G. et al. DNA-based artificial signaling system mimicking the dimerization of receptors for signal transduction and amplification. *Anal. Chem.* **93**, 13807–13814 (2021).
73. Qian, L., Soloveichik, D. & Winfree, E. Efficient turing-universal computation with DNA polymers BT - DNA computing and molecular programming; Sakakibara, Y., Mi, Y., Eds.; Springer Berlin Heidelberg: Berlin, Heidelberg, 2011; pp 123–140.
74. Liu, M. et al. A DNA tweezer-actuated enzyme nanoreactor. *Nat. Commun.* **4**, 2127 (2013).
75. Fu, J. et al. DNA-scaffolded proximity assembly and confinement of multienzyme reactions. *Top. Curr. Chem.* **378**, 38 (2020).
76. Trinh, T., Chidchob, P., Bazzi, H. S. & Sleiman, H. F. DNA micelles as nanoreactors: efficient DNA functionalization with hydrophobic organic molecules. *Chem. Commun.* **52**, 10914–10917 (2016).
77. Li, T. et al. Reprogramming bacterial protein organelles as a nanoreactor for hydrogen production. *Nat. Commun.* **11**, 5448 (2020).
78. Jia, W. et al. Programmable nano-reactors for stochastic sensing. *Nat. Commun.* **12**, 5811 (2021).
79. Comellas-Aragonès, M. et al. A virus-based single-enzyme nanoreactor. *Nat. Nanotechnol.* **2**, 635–639 (2007).
80. Bolinger, P.-Y., Stamou, D. & Vogel, H. Integrated nanoreactor systems: triggering the release and mixing of compounds inside single vesicles. *J. Am. Chem. Soc.* **126**, 8594–8595 (2004).
81. Man, T. et al. Hierarchically encapsulating enzymes with multi-shelled metal-organic frameworks for tandem biocatalytic reactions. *Nat. Commun.* **13**, 305 (2022).
82. Vriezema, D. M. et al. Positional assembly of enzymes in polymer-some nanoreactors for cascade reactions. *Angew. Chem. Int. Ed.* **46**, 7378–7382 (2007).
83. Pandey, S. et al. Zeptoliter DNA origami reactor to reveal cosolute effects on nanoconfined g-quadruplexes. *J. Phys. Chem. Lett.* **13**, 8692–8698 (2022).
84. Zhao, Z. et al. Nanocaged enzymes with enhanced catalytic activity and increased stability against protease digestion. *Nat. Commun.* **7**, 10619 (2016).
85. Linko, V., Eerikainen, M. & Kostianen, M. A. A modular DNA origami-based enzyme cascade nanoreactor. *Chem. Commun.* **51**, 5351–5354 (2015).
86. Antonny, B. Mechanisms of membrane curvature sensing. *Annu. Rev. Biochem.* **80**, 101–123 (2011).

87. Has, C., Sivadas, P. & Das, S. L. Insights into membrane curvature sensing and membrane remodeling by intrinsically disordered proteins and protein regions. *J. Membr. Biol.* **255**, 237–259 (2022).
88. Bunge, A. et al. Lipophilic oligonucleotides spontaneously insert into lipid membranes, bind complementary DNA strands, and sequester into lipid-disordered domains. *Langmuir* **23**, 4455–4464 (2007).
89. Rubio-Sánchez, R., Barker, S. E., Walczak, M., Cicuta, P. & Michele, L. D. A modular, dynamic, DNA-based platform for regulating cargo distribution and transport between lipid domains. *Nano Lett.* **21**, 2800–2808 (2021).
90. Li, C.-L., Xue, D.-X., Wang, Y.-H., Xie, Z.-P. & Staehelin, C. A method for functional testing constitutive and ligand-induced interactions of lysin motif receptor proteins. *Plant Methods* **16**, 3 (2020).
91. Wickham, S. F. J. et al. Complex multicomponent patterns rendered on a 3D DNA-barrel pegboard. *Nat. Commun.* **11**, 5768 (2020).
92. Agasti, S. S., Liong, M., Peterson, V. M., Lee, H. & Weissleder, R. Photocleavable DNA barcode–antibody conjugates allow sensitive and multiplexed protein analysis in single cells. *J. Am. Chem. Soc.* **134**, 18499–18502 (2012).
93. Douglas, S. M. et al. Rapid prototyping of 3D DNA-origami shapes with CaDNAo. *Nucleic Acids Res.* **37**, 5001–5006 (2009).
94. Castro, C. E. et al. A primer to scaffolded DNA origami. *Nat. Methods* **8**, 221–229 (2011).
95. Turner, P. J. XMGRACE, Version 5.1. 19.Center for Coastal and Land-Margin Research, Oregon Graduate Institute of Science and Technology. (Beaverton, OR 2005).

Acknowledgements

V.M. acknowledges Erik Winfree and Lulu Qian for both their comments and access to equipment for initial experiments. V.M. thanks Human Frontier Science Program (HFSP LT001164/2017-L) for a Postdoctoral Fellowship and Caltech for additional support. This study was supported by the National Institute of Mental Health awards MH125320 (to P.W.K.R. and E.R.C.), MH061876 and NS097362 (to E.R.C.), and by the National Science Foundation awards CCF 2106695 (to C.T.), a Faculty Early Career Development Award CCF 2143227 (to C.T.) and a Future Manufacturing award MCB 2134772 (to P.W.K.R.). E.R.C. is an investigator at the Howard Hughes Medical Institute (HHMI). This article is subject to HHMI's Open Access to Publications policy. HHMI lab heads have previously granted a nonexclusive CC BY 4.0 license to the public and a sublicensable license to HHMI in their research articles. Pursuant to those licenses, the author-accepted manuscript of this article can be made freely available under a CC BY 4.0 license immediately upon publication.

Author contributions

V.M. conceived the original idea, designed, performed, and analyzed most experiments, and wrote the manuscript's first draft. V.M., Z.Z., C.T.,

and P.W.K.R. contributed further ideas. C.T., V.M., and P.W.K.R. designed the DNA logic circuit and analyzed kinetics data. Z.Z. designed the origami, assisted in DOL synthesis, and performed TEM. N.S. and C.T. modeled the DNA circuit. E.R.C. mentored and hosted V.M. All authors discussed the results and participated in manuscript writing.

Competing interests

Certain aspects related to the internal immobilization and the release of membrane receptors employing DNA origami are covered in a pending US provisional patent application (63/415,546) owned by the California Institute of Technology with inventor V.M. The other authors declare no competing interests.

Additional information

Supplementary information The online version contains supplementary material available at <https://doi.org/10.1038/s41467-023-36996-x>.

Correspondence and requests for materials should be addressed to Vishal Maingi, Chris Thachuk, Edwin R. Chapman or Paul W. K. Rothmund.

Peer review information *Nature Communications* thanks Jianbo Liu and the other anonymous reviewer(s) for their contribution to the peer review of this work.

Reprints and permissions information is available at <http://www.nature.com/reprints>

Publisher's note Springer Nature remains neutral with regard to jurisdictional claims in published maps and institutional affiliations.

Open Access This article is licensed under a Creative Commons Attribution 4.0 International License, which permits use, sharing, adaptation, distribution and reproduction in any medium or format, as long as you give appropriate credit to the original author(s) and the source, provide a link to the Creative Commons license, and indicate if changes were made. The images or other third party material in this article are included in the article's Creative Commons license, unless indicated otherwise in a credit line to the material. If material is not included in the article's Creative Commons license and your intended use is not permitted by statutory regulation or exceeds the permitted use, you will need to obtain permission directly from the copyright holder. To view a copy of this license, visit <http://creativecommons.org/licenses/by/4.0/>.

© The Author(s) 2023